Naval Research Laboratory

Washington, DC 20375-5320

NRL/MR/6793--95-7639

Theory of Competition between Synchronous and Nonsynchronous Modes in a Magnicon Output Cavity

ARNE W. FLIFLET
STEVEN H. GOLD

Beam Physics Branch
Plasma Physics Division

DTIC
ELECTE
MAR 15 1995
S G D

March 16, 1995

19950313 018

Approved for public release; distribution unlimited.

REPORT DOCUMENTATION PAGE

Form Approved
OMB No. 0704-0188

Public reporting burden for this collection of information is estimated to average 1 hour per response, including the time for reviewing instructions, searching existing data sources, gathering and maintaining the data needed, and completing and reviewing the collection of information. Send comments regarding this burden estimate or any other aspect of this collection of information, including suggestions for reducing this burden, to Washington Headquarters Services, Directorate for Information Operations and Reports, 1215 Jefferson Davis Highway, Suite 1204, Arlington, VA 22202-4302, and to the Office of Management and Budget. Paperwork Reduction Project (0704-0188), Washington, DC 20503.

1. AGENCY USE ONLY *(Leave Blank)*	2. REPORT DATE	3. REPORT TYPE AND DATES COVERED
	March 16, 1995	Interim Report

4. TITLE AND SUBTITLE

Theory of Competition between Synchronous and Nonsynchronous Modes in a Magnicon Output Cavity

5. FUNDING NUMBERS

DE-AI02-94ER40861.A000

6. AUTHOR(S)

Arne W. Fliflet and Steven H. Gold

7. PERFORMING ORGANIZATION NAME(S) AND ADDRESS(ES)

Naval Research Laboratory
Washington, DC 20375-5320

8. PERFORMING ORGANIZATION REPORT NUMBER

NRL/MR/6793--95-7639

9. SPONSORING/MONITORING AGENCY NAME(S) AND ADDRESS(ES)

Office of Naval Research, Arlington, VA
Department of Energy, Washington, DC

10. SPONSORING/MONITORING AGENCY REPORT NUMBER

11. SUPPLEMENTARY NOTES

12a. DISTRIBUTION/AVAILABILITY STATEMENT

Approved for public release; distribution unlimited.

12b. DISTRIBUTION CODE

13. ABSTRACT *(Maximum 200 words)*

In the magnicon amplifier, a scanning electron beam drives a synchronous fast-wave interaction in a gyrotron-like output cavity. The output cavity is designed to support the synchronous TM_{210} operating mode. However, a number of other TE or TM modes can be excited in the cavity via a nonsynchronous, gyrotron-type interaction. To investigate the possibility of competition from these nonsynchronous modes, a multimode gyrotron simulation theory and code have been adapted to the magnicon configuration. The gyrotron theory and corresponding code have been generalized to include a synchronous TM mode as well as nonsynchronous TE modes. Proper phase averaging between the modes, and between the modes and the beam electrons, is critical to accurate mode competition calculations. In nonsynchronous interactions this is achieved by averaging with respect to electron entrance time and the orbit guiding center angle. The synchronous mode interaction is invariant with respect to these two averages; however, it is affected by scanning angle spread which is included via a third average over scanning angles. Calculations have been carried out to model a second-harmonic X-Band magnicon experiment which is currently underway at the Naval Research Laboratory (NRL). The output cavity has been optimized for the TM_{210} mode at 11.4 GHz or twice the drive frequency (ω_d = 5.7 GHz). The principal competing mode is the TE_{121} mode. The simulations show that nonsynchronous mode interactions are suppressed by the synchronous interaction if the scanning angle spread is sufficiently small ($\leq 90°$ in the NRL configuration).

14. SUBJECT TERMS

Magnicon synchronous interaction
Multi-mode
Simulation
Gyrotron
Maser

15. NUMBER OF PAGES

22

16. PRICE CODE

17. SECURITY CLASSIFICATION OF REPORT	18. SECURITY CLASSIFICATION OF THIS PAGE	19. SECURITY CLASSIFICATION OF ABSTRACT	20. LIMITATION OF ABSTRACT
UNCLASSIFIED	UNCLASSIFIED	UNCLASSIFIED	UL

NSN 7540-01-280-5500

Standard Form 298 (Rev. 2-89)
Prescribed by ANSI Std 239-18
298-102

CONTENTS

I. INTRODUCTION 1

II. THEORY 2

III. CALCULATIONS AND RESULTS 8

IV. DISCUSSION AND CONCLUSIONS 11

V. ACKNOWLEDGMENT 11

REFERENCES 12

Accesion For

NTIS CRA&I ☒
DTIC TAB ☐
Unannounced ☐
Justification .....

By .....
Distribution /

Availability Codes

Dist	Avail and / or Special
A-1	

THEORY OF COMPETITION BETWEEN SYNCHRONOUS AND NONSYNCHRONOUS MODES IN A MAGNICON OUTPUT CAVITY

I Introduction

The magnicon is under development as an efficient, high-power microwave amplifier for powering the next generation of electron accelerators for high energy physics research.[1-10] These accelerators are expected to operate at several times the frequencies currently in use, i.e., X-Band or above. This will require a significant advance in the performance of high power amplifiers in this frequency regime. The magnicon is based on a scanning electron beam that is obtained by passing a magnetized pencil beam from a Pierce-type electron gun through a radio-frequency (RF) field deflection system. A schematic of the magnicon is shown in Fig. 1. The deflection system consists of a series of cavities—the first one driven externally—each of which support a rotating transverse magnetic (TM) waveguide mode, namely, the TM_{110} mode, at $\sim 1/2$ the cyclotron frequency. The deflection system produces a gyrating beam with high transverse momentum, i.e. $\alpha = v_\perp/v_{||} \geq 1$, where $v_\perp$ and $v_{||}$ are the transverse and axial components of the electron beam velocity. The beam drives a gyrotron-like interaction in the output cavity; however, unlike the conventional phase-mixed gyrotron electron beam, at the cavity entry point the beam centroid rotates, or "scans" about the cavity axis at the drive frequency ω_d. The output cavity is designed such that the operating mode frequency ω satisfies the synchronism condition $\omega = M\omega_d$, where M is the azimuthal index of the mode. In this case the electron beam entry point rotates synchronously with the cavity RF fields, so that an ideal pencil beam interacts as a single electron, resulting in a highly efficient interaction. The nonlinear efficiency of the magnicon output cavity operating in the TM_{210} has been investigated by Hafizi *et al.*[7,11]. In this paper, the possibility of mode competition in the magnicon output cavity, an important factor in the operation of other gyro-devices, is investigated. In general, the overmoded output cavity supports other transverse electric (TE) and TM modes, some of which will have frequencies near the operating frequency. For these nonsynchronous modes, the beam entrance gyro-phase is completely randomized and the beam drives a conventional gyrotron interaction. Nevertheless, depending on the mode output coupling and transverse structure, these modes

Manuscript approved December 14, 1994

may have low threshold currents and thus represent potential competing modes. For a nonideal magnicon beam, competition from nonsynchronous modes will be affected by scanning angle spread, which degrades the the interaction with the synchronous mode. In fact, when the scanning angle spread reaches $2\pi/M$ the magnicon interaction is identical to the gyrotron interaction.

In this work, a time-dependent, multimode gyrotron theory and associated computer code[12,13] have been modified to examine competition in the output cavity between the phase-synchronous operating mode and the other nonsynchronous modes which interact via the conventional gyrotron interaction. Calculations have been carried out to model a second-harmonic X-Band magnicon experiment which is currently under way at the Naval Research Laboratory (NRL). The output cavity has been optimized for the TM_{210} mode at 11.4 GHz or twice the drive frequency ($\omega_d = 5.7$ GHz). The principal competing mode is the TE_{121} mode. A nonlinear theory for these modes is developed in the next section. Generalization to several modes is straight forward. The results of calculations are given in Section III and our conclusions are given in Section IV.

II Theory

A time-dependent multimode theory of gyrotron oscillators has been developed in previous work.[12,13] A summary of the approach is given here with emphasis on the new features in the analysis, including the synchronous interaction with a TM mode. Consider a cylindrical magnicon output cavity which is tuned for a synchronous interaction with a $TM_{MN\ell}$ mode at the angular frequency ω. After passing through the deflection cavities, the beam electrons follow helical trajectories with respect to guiding centers which are distributed such that at the entrance to the output cavity, the beam position rotates or "scans" at the drive frequency ω_d. The operating mode satisfies the synchronism condition $\omega = M\omega_d$. In addition to the synchronous mode interaction, the beam interacts with a nonsynchronous mode, which is assumed to be a TE_{mn1} mode, although in general there could be interactions with more than one nonsynchronous TE or TM mode. The electron beam geometry

is shown in Fig. 2. The RF fields in the output cavity can be represented by the vector potential:

$$\vec{A}(\vec{r},t) = \vec{A}_{\rm m}(\vec{r},\omega,t) + \vec{A}_{\rm g}(\vec{r},\omega_{\rm g},t) \tag{1}$$

where $\vec{A}_{\rm m}$ corresponds to the synchronous TM mode and is given by:

$$A_{\rm m||}(\vec{r},\omega,t) = {\rm Re}\left\{\left(\frac{\omega_{co}}{\omega}\right)^2 a_{\rm m}(t)\, g(z)\, \psi_{MN}^{TM}(r,\theta) \exp\left[-i\left(\omega t + \xi_{\rm m}(t)\right)\right]\right\} \tag{2}$$

$$\vec{A}_{\rm m\perp}(\vec{r},\omega,t) = -{\rm Re}\left\{\frac{c}{\omega^2} a_{\rm m}(t) \frac{dg}{dz}\vec{b}(r,\theta) \exp\left[-i\left(\omega t + \xi_{\rm m}(t)\right)\right]\right\} \tag{3}$$

where ω_{co} is the cutoff frequency of the $\mathrm{TM}_{MN\ell}$ mode, $\vec{b} = -\nabla_t \psi_{MN}^{TM}$ is the transverse vector mode function for a TM mode, $\psi_{MN}^{TM}(r,\theta) = C_{MN}^{TM} {\rm J}_M(k_{MN} r)\exp(iM\theta)$ is the cylindrical waveguide scalar function, and $a_{\rm m}(t)$ and $\xi_{\rm m}(t)$ are slowly varying amplitude and phase factors which satisfy $\partial\xi_{\rm m}/\partial t << \omega\xi_{\rm m}$. The normalization coefficient of the scalar function is: $C_{MN}^{\rm TM} = 1/\left(\sqrt{\pi} x_{MN} J'_M(x_{MN})\right)$, ${\rm J}_M$ is a Bessel function of the first kind, ${\rm J}'_M(x) = d{\rm J}_M(x)/dx$, and $k_{MN} = x_{MN}/r_{\rm w}$ is the transverse wavenumber of the magnicon mode where x_{MN} is the nth zero of ${\rm J}_M$.[14] The mode axial profile is given by the function g. The TE mode vector potential is purely transverse and is given by:

$$\vec{A}_{\rm g}(\vec{r},\omega_{\rm g},t) = {\rm Re}\left\{\frac{1}{i\omega_{\rm g}} a_{\rm g}(t)\, h(z)\, \vec{e}_{mn} \exp\left[-i\left(\omega_{\rm g} t + \xi_{\rm g}(t)\right)\right]\right\} \tag{4}$$

where $\vec{e}_{mn} = \hat{z} \times \nabla_t \Psi_{mn}^{TE}$ is the waveguide transverse-mode vector function for a TE mode, and h is the axial profile function. The TE mode scalar function is given by: $\psi_{mn}^{\rm TE}(r,\theta) = C_{mn}^{\rm TE} {\rm J}_M(k_{mn} r)\exp(im\theta)$, the normalization coefficient is given by: $C_{mn}^{\rm TE} = 1/\left(\sqrt{\pi\left(x'^2_{mn} - m^2\right)}{\rm J}_m\left(x'_{mn}\right)\right)$, $\omega_{\rm g}$ is the frequency of the competing gyrotron mode, and $k_{mn} = x_{mn}/r_{\rm w}$ is the TE mode transverse wavenumber where x'_{mn} is the nth zero of ${\rm J}'_m$. The rf-field components are obtained from the vector potential using $\vec{E} = -\partial\vec{A}/\partial t$ and $\vec{B} = \nabla \times \vec{A}$. Rate equations for the slow-time-scale mode amplitudes and phases can be derived by substituting the above expressions for the components of $\vec{A}$ into the wave equation:

$$\nabla^2 \vec{A} - \frac{1}{c^2}\frac{\partial^2 \vec{A}}{\partial t^2} = \mu_0 \vec{J} \tag{5}$$

where $\vec{J}$ is the electron beam alternating current (AC) current density, c is the speed of light, and μ_0 is the permeability of free space. SI units are used throughout except as noted. The result is:

$$\frac{da_{\rm m}}{dt} + \frac{\omega a_{\rm m}}{2Q_{\rm m}} = -\frac{Z_0 c}{2}{\rm Im}\mathcal{Q}(t) \tag{6}$$

$$\frac{d\xi_{\rm m}}{dt} = -\frac{Z_0 c}{2a_{\rm m}}{\rm Re}\mathcal{Q}(t) \tag{7}$$

$$\frac{da_{\rm g}}{dt} + \frac{\omega_{\rm g} a_{\rm g}}{2Q_{\rm g}} = -\frac{Z_0 c}{2}{\rm Im}\mathcal{P}(t) \tag{8}$$

$$\frac{d\xi_{\rm g}}{dt} = -\frac{Z_0 c}{2a_{\rm g}}{\rm Re}\mathcal{P}(t) \tag{9}$$

where $Z_0 = 377$ ohms is the free-space impedance,

$$\mathcal{P}(t) = \frac{i}{W_{\rm g}}\frac{1}{2\pi}\int_0^{2\pi} d(\omega_{\rm g} t)\int_V da\ dz\ h(z)\vec{e}_{\rm g}^{\,*}\cdot\vec{J}_t e^{i(\omega_{\rm g} t+\xi_{\rm g})}, \tag{10}$$

and

$$\mathcal{Q}(t) = \frac{i}{W_{\rm m}}\frac{1}{2\pi}\int_0^{2\pi} d(\omega t)\int_V da\ dz\ g(z)\psi_{MN}^{\rm TM} J_z e^{i(\omega t+\xi_{\rm m})}. \tag{11}$$

The mode axial normalization integrals are given by:

$$W_{\rm g} = \int_0^L dz\,|h(z)|^2, \tag{12}$$

and

$$W_{\rm m} = \int_0^L dz\,|g(z)|^2. \tag{13}$$

In this work, only the lowest order axial modes are considered. A sinusoidal profile will be assumed for h and g is assumed to be constant, i.e., $h(z) = \sin(k_z z)$ where $k_z = \pi/L$ and $g = 1$. These choices are appropriate for a closed cylindrical cavity. Performing the integrals in Eqs.(12) and (13) lead to $W_{\rm g} = L/2$ and $W_{\rm m} = L$.

The value of the mode excitation functions $\mathcal{P}$ and $\mathcal{Q}$ at the time t depends on the motion of electrons which entered the cavity between the times t and $t - L/v_z$. Thus the mode rate equations are nonlocal integro-differential equations. To calculate the AC current density, the interaction with the electron beam is treated in the single-particle approximation. The general time-dependent problem can be simplified by using the fact

that the characteristic rise-time of fields in the resonator is much longer than the electron transit time in the cavity as well as the wave period. In this case, one can use a quasi-steady-state approximation in which the electron trajectories are calculated for rf modes with fixed amplitude. Neglecting space-charge effects and guiding center drifts, the slow-time-scale nonlinear equations-of-motion for an electron with guiding center coordinates (R_0, Θ_0) immersed in an axial magnetic field B_0 and interacting at a particular harmonic with a synchronous TM mode and a nonsynchronous TE mode are readily deduced from previous steady-state, single-mode analyses,[14,15,16] and are given by:

$$\begin{aligned}\frac{du_t}{d\bar{z}} &= -\frac{\gamma}{u_z} f_{\mathrm{m}} \frac{s}{\bar{k}_{MN}\bar{r}_L} \mathrm{J}_s\left(\bar{k}_{MN}\bar{r}_L\right) \mathrm{Re}\left\{\left(\frac{1}{\bar{\omega}}\frac{dg}{d\bar{z}} - i\frac{u_z}{\gamma}g\right)\exp\left[-i\left(\Lambda+\xi_{\mathrm{m}}\right)\right]\right\}, \\ &\quad -\frac{\gamma}{u_z} f_{\mathrm{g}} \mathrm{J}'_s\left(\bar{k}_{mn}\bar{r}_L\right) \mathrm{Re}\left\{\left(h + i\frac{u_z}{\gamma\bar{\omega}_{\mathrm{g}}}\frac{dh}{d\bar{z}}\right)\exp\left[-i\left(\Lambda+\Xi_{\mathrm{g}}\right)\right]\right\} \qquad (14)\end{aligned}$$

$$\begin{aligned}\frac{d\Lambda}{d\bar{z}} &= \frac{\gamma\bar{\omega}}{u_{\|}}\left(1 - \frac{s\bar{\Omega}\gamma_0}{\bar{\omega}\gamma}\right) - \frac{s\gamma}{u_z u_t} f_{\mathrm{m}} \mathrm{J}'_s\left(\bar{k}_{MN}\bar{r}_L\right) \mathrm{Re}\left\{\left(\frac{1}{\bar{\omega}}\frac{dg}{d\bar{z}} - i\frac{u_z}{\gamma}g\right)\exp\left[-i\left(\Lambda+\xi_{\mathrm{m}}\right)\right]\right\} \\ &\quad + \frac{s\gamma}{u_z u_t} f_{\mathrm{g}} \frac{s\mathrm{J}_s\left(\bar{k}_{mn}\bar{r}_L\right)}{\bar{k}_{mn}\bar{r}_L} \mathrm{Re}\left\{i\left(h + i\frac{u_z}{\gamma\bar{\omega}_{\mathrm{g}}}\frac{dh}{d\bar{z}} - \frac{\omega_{\mathrm{gco}}^2 u_t^2}{s\Omega\omega_{\mathrm{g}}\gamma}h\right)\exp\left[-i\left(\Lambda+\Xi_{\mathrm{g}}\right)\right]\right\} \qquad (15)\end{aligned}$$

$$\begin{aligned}\frac{du_z}{d\bar{z}} &= \frac{u_t}{u_z}\left(\frac{\gamma\omega_{\mathrm{co}}^2}{s\gamma_0\omega\Omega} - 1\right) f_{\mathrm{m}} \frac{s\mathrm{J}_s\left(\bar{k}_{MN}\bar{r}_L\right)}{\bar{k}_{MN}\bar{r}_L} \mathrm{Re}\left\{ig\exp\left[-i\left(\Lambda+\xi_{\mathrm{m}}\right)\right]\right\} \\ &\quad + \frac{u_t}{u_z\bar{\omega}} f_{\mathrm{g}} \mathrm{J}'_s\left(\bar{k}_{mn}\bar{r}_L\right) \mathrm{Re}\left\{i\frac{dh}{d\bar{z}}\exp\left[-i\left(\Lambda+\Xi_{\mathrm{g}}\right)\right]\right\} \qquad (16)\end{aligned}$$

where $u_t = \gamma v_t/c$ is the normalized transverse momentum amplitude, $u_z = \gamma v_z/c$ is the normalized axial momentum (v_t and v_z denote the electron transverse and axial velocities, respectively),

$$\Lambda(z) = (\omega - s\Omega)\, z/v_z - s\phi + \omega t_0 - (M - s)\,\Theta_0 \qquad (17)$$

gives the slow variation in the transverse momentum phase relative to the reference wave phase, and

$$\Xi_{\mathrm{g}} = \xi_{\mathrm{g}} + (\omega_{\mathrm{g}} - \omega)z/v_{\|} + (\omega_{\mathrm{g}} - \omega)\, t_0 - (m - M)\,\Theta_0. \qquad (18)$$

Other variables denote: s, the harmonic number, γ (γ_0), the (initial) relativistic mass ratio

which is given by:

$$\gamma = \left(1 + u_t^2 + u_z^2\right)^{1/2}, \tag{19}$$

r_L, the Larmor radius of the orbit, Ω, the relativistic cyclotron frequency of the unperturbed beam, and $f_{\rm m}$ and $f_{\rm g}$, the normalized TM and TE mode amplitudes given by:

$$f_{\rm m} = \frac{|e|}{m_0 c} x_{MN} C_{MN}^{\rm TM} {\rm J}_{M-s}\left(k_{MN} R_0\right) a_{\rm m}(t_0) \tag{20}$$

$$f_{\rm g} = \frac{|e|}{m_0 c^2} x'_{mn} C_{mn}^{\rm TE} {\rm J}_{m-s}\left(k_{mn} R_0\right) a_{\rm g}(t_0) \tag{21}$$

Quantities with an overbar have been normalized according to: $\bar{z} = z/r_{\rm w}$, $\bar{r}_L = r_L/r_{\rm w}$, $\bar{\Omega} = \Omega r_{\rm w}/c$, $\bar{\omega} = \omega r_{\rm w}/c$, and $\bar{k}_{mn} = k_{mn} r_{\rm w}$. R_0 and Θ_0 denote the electron orbit guiding center radius and azimuthal angle, $|e|$ is the electron charge, m_0 is the electron rest mass, $r_{\rm w}$ is an arbitrary normalization radius, and ϕ gives the slow variation in the transverse momentum phase relative to the cyclotron motion. At the cavity entrance, the transverse momentum phase parameter is given by

$$\Lambda(0) = -s\phi_0 + \omega t_0 - (M - s)\,\Theta_0, \tag{22}$$

where $\phi_0 = \phi(z = 0)$ is the electron gyrophase at the cavity entrance. For a magnicon scanning electron beam,

$$\phi_0 = \theta_{\rm sc} + c_1 \tag{23}$$

$$\Theta_0 = \theta_{\rm sc} + c_2, \tag{24}$$

where c_1 and c_2 are constants and the scanning angle is given by:

$$\theta_{\rm sc} = \omega_{\rm d} t_0 + \theta_{\rm sc0}. \tag{25}$$

The angle $\theta_{\rm sc0}$ accounts for the spread in scanning angles resulting from a nonideal beam formation system. Substituting Eqs. (23) and (24) into Eq. (22) and using Eq. (25) leads to:

$$\Lambda(0) = \Lambda_0 - M\theta_{\rm sc0} \tag{26}$$

where Λ_0 is an overall phase constant, which may set to zero without loss of generality.

The AC current density is obtained by integrating Eqs.(14)–(16) for an appropriate set of initial conditions at the cavity input $z = 0$. The AC current density is given by:

$$\vec{J} = -\frac{I_0}{v_z}\vec{v}. \tag{27}$$

Using the prescription developed in previous work,[15] Eqs.(8) and (9) for the mode amplitude and phase can be rewritten as:

$$\frac{df_{\rm m}}{d\tau} = -\frac{f_{\rm m}}{2Q_{\rm m}} + \tilde{I}_{\rm m}\int_0^{\bar{L}} d\bar{z}g(\bar{z})\left\langle \mathrm{J}_s(k_{MN}r_L)\frac{u_t}{u_z}\sin\left[\Lambda+\xi_{\rm m}\right]\right\rangle_{\theta_{sc0},\Theta_0,t_0} \tag{28}$$

$$\frac{d\xi_{\rm m}}{d\tau} = -\frac{\tilde{I}_{\rm m}}{f_{\rm m}}\int_0^{\bar{L}} d\bar{z}\ g(\bar{z})\left\langle \mathrm{J}_s(k_{mn}r_L)\frac{u_t}{u_z}\cos\left[\Lambda+\xi_{\rm m}\right]\right\rangle_{\theta_{sc0},\Theta_0,t_0} \tag{29}$$

$$\frac{df_{\rm g}}{d\tau} = -\frac{\omega_{\rm g}}{\omega}\frac{f_{\rm g}}{2Q_{\rm g}} + \tilde{I}_{\rm g}\int_0^{\bar{L}} d\bar{z}h(\bar{z})\left\langle \mathrm{J}'_s(k_{mn}r_L)\frac{u_t}{u_z}\cos\left[\Lambda+\Xi_{\rm g}\right]\right\rangle_{\theta_{sc0},\Theta_0,t_0} \tag{30}$$

$$\frac{d\xi_{\rm g}}{d\tau} = -\frac{\tilde{I}_{\rm g}}{f_{\rm g}}\int_0^{\bar{L}} d\bar{z}\ h(\bar{z})\left\langle \mathrm{J}'_s(k_{mn}r_L)\frac{u_t}{u_z}\sin\left[\Lambda+\Xi_{\rm g}\right]\right\rangle_{\theta_{sc0},\Theta_0,t_0} \tag{31}$$

where $\tau = \omega t$; $\langle\ \rangle_{\theta_{sc0},\Theta_0,t_0}$ denotes the average with respect to the initial scanning angles, guiding center angles, and cavity entrance times of the electrons; and $\bar{L}$ is the normalized interaction length. The normalized current factors are given by:

$$\tilde{I}_{\rm m} = \frac{|e|Z_0}{m_0c^2\bar{\omega}}\frac{\mathrm{J}^2_{M-s}(k_{MN}R_0)}{\pi \mathrm{J}'^2_M(x_{MN})\bar{W}_{\rm m}}I_0 \tag{32}$$

$$\tilde{I}_{\rm g} = \frac{|e|Z_0}{m_0c^2\bar{\omega}}\frac{\mathrm{J}^2_{m-s}(k_{mn}R_0)}{\pi\left(1-m^2/x'^2_{mn}\right)\mathrm{J}^2_m(x'_{mn})\bar{W}_{\rm g}}I_0 \tag{33}$$

where I_0 is the DC beam current. The numerical calculations can be greatly simplified for low-order harmonic interactions by noting that the Bessel functions J_s and J'_s which occur in the equations-of-motion and the rate equations for the mode amplitude and phase source terms can be replaced by their small argument expansions with little loss of accuracy.

The time-dependent simulation is initiated by assigning a small initial amplitude and arbitrary phase to a set of modes which may participate in the interaction. The corresponding induced AC current density is obtained by integrating the equations-of-motion [Eqs.(14)–(16)], and is used to construct the source terms in Eqs.(28)–(31). Eqs.(28)–(31) can then

be integrated a single time step and the process repeated. The initial conditions for the equations-of-motion for the magnicon scanning electron beam are: $u_t(0) = u_{t_0}, u_z(0) = u_{z_0}$, a fixed guiding-center radius R_0, Θ_0 is uniformly distributed in the interval $[0, 2\pi]$, t_0 is averaged over the longest beat-wave period of the modes present in the cavity, and a certain spread in angles is assumed for θ_{sc0}. The interaction efficiency is given by:

$$\eta = \frac{\gamma_0 - \langle \gamma\,(z = L)\rangle_{\theta_{sc0},\Theta_0,t_0}}{\gamma_0 - 1} \tag{34}$$

The output power in a TM mode is given by:

$$P_{\rm m}(\tau) = \frac{\pi m_0^2 c^4}{2Z_0 e^2} \frac{\mathrm{J}'^2_M(x_{MN})}{Q_{\rm m}\mathrm{J}^2_{M-s}(k_{MN}R_0)} \bar{\omega}\bar{W}_{\rm m}\,|f_{\rm m}(\tau)|^2 \tag{35}$$

and the power in a TE mode is given by:

$$P_{\rm g}(\tau) = \frac{\pi m_0^2 c^4}{2Z_0 e^2} \frac{(1 - m^2/x'^2_{mn})\,\mathrm{J}^2_m(x'_{mn})}{Q_{\rm g}\mathrm{J}^2_{m-s}(k_{mn}R_0)} \bar{\omega}_{\rm g}\bar{W}_{\rm g}\,|f_{\rm g}(\tau)|^2 \tag{36}$$

III Calculations and Results

The magnicon parameters were obtained in a previous optimization study carried out for the NRL experimental configuration.[7] The electron beam energy and current are 500 kV and 172 A. The beam pitch ratio after transiting the deflection cavities is $\alpha = 1.0$. An ideal cylindrical output cavity is assumed with a radius of 2.145 cm and a length of 5 cm. The effect of the beam tunnel apertures is neglected. The TM_{210} operating mode Bessel function zero $x_{21} = 5.135$ and the cold-cavity oscillation frequency is 11.42 GHz. For simplicity in legislating the synchronism condition, frequency shifts due to beam loading ($\sim$ 1 MHz) have been neglected in the mode rate equation source terms and in the equations-of-motion. This allows the drive frequency to be set equal to the cold-cavity frequency. The mode phase time dependence resulting from these shifts has been calculated. Possible near-cutoff, nonsynchronous competing modes include the TM_{020} mode ($x_{02} = 5.520$ and $f = 12.27$ GHz), the TE_{411} mode ($x'_{41} = 5.320$ and $f = 12.20$ GHz), and the TE_{121} mode

($x'_{12} = 5.33$ and $f = 12.23$ GHz). Of these, the most dangerous competing mode is the TE_{121} mode because its fields are peaked on axis and therefore couple strongly to the beam which propagates near the axis. In the slow-time-scale approximation, the coupling strength of the TM_{210} operating mode is proportional to $J_1^2(2.39R_0)$ whereas that of the TE_{121} mode is proportional to $J_0^2(2.49R_0)$. Thus the relative coupling strength of these modes is strongly affected by the electron beam guiding center radius, i.e., near the axis an increase in beam radius increases the coupling to the TM_{210} mode while decreasing the coupling to the TE_{121} mode. In this study a guiding center radius $R_0 = 0.45$ cm was chosen. This value optimizes the efficiency of the TM_{210} mode in the slow-time-scale approximation for the chosen cavity and beam parameters, and is consistent with simulation results for the size of the NRL electron beam after passing through the deflection cavities. The oscillation threshold currents of the TE_{121} and TM_{210} modes were calculated numerically by integrating the equations-of-motion in the small signal regime and are shown in Fig. 3 as a function of the applied magnetic field for a Q-factor of 200. The threshold current of TE_{121} mode is about half the operating current so that high power oscillation is expected unless it is suppressed by the synchronous mode. Conversely, the threshold current of the TM_{210} mode for a phase-mixed beam is greater than the beam current, as shown in Fig. 3.

Competition between the synchronous TM_{210} mode and the nonsynchronous TE_{121} was investigated using the formalism presented in the preceding section. The numerical integrations were carried out using a fourth-order Runga-Kutta algorithm for both the field rate equations and the equations of motion.[17] Twelve phases were used in each of the averages over Θ_0, θ_{sc0}, and t_0. Fifty points were used in the equation-of-motion integrations through the cavity. The results were found to be insensitive to increasing the number of points used in these averages and integrations.

The time evolution of the output power in the TM_{210} synchronous mode and the TE_{121} gyrotron mode is shown in Fig. 4 for scanning angle spreads of 45° and 90°. A uniform (top hat) distribution of particles was used to model the spread. A 20 ns voltage ramp, in which the initial voltage was 0.8 of the maximum, was used to model effects of a finite voltage

risetime, however, the results were not affected by this ramp. This is in contrast to the case of mode competition in gyrotron oscillators where a voltage ramp can affect the multimode equilibrium state by varying the mode detunings during start-up.[13] In the present case the voltage ramp increased the initial growth rate of the TE_{121} mode but had little effect on the much faster growth rate of the TM_{210} synchronous mode. The maximum beam current and beam velocity pitch ratio were used from the beginning of the simulations. For both values of scanning angle spread, the nonsynchronous mode is suppressed by the magnicon interaction, but the suppression is weaker for the larger scanning-angle spread. Our calculations indicate that there are two basic effects of increasing scanning angle spead. The first is a reduction in the operating mode efficiency and the second is a weakening in the ability of the synchronous mode to suppress the nonsynchronous competing mode. Both these effects are illustrated in Fig. 4. At a particular spread value, which depends on the beam size, the latter is no longer completely suppressed and a multimode equilibrium results. Such a case is shown in Fig. 5. This figure shows the time evolution of the TM_{210} mode normalized axial electric field and the TE_{121} mode normalized transverse electric field for a large scanning-angle spread of 122°. The voltage profile is also shown. In this case the TE mode is not suppressed, but has a reduced growth rate. It eventually grows to large amplitude and partially suppresses the TM_{210} mode forming a multimode equilibrium. Fig. 6 summarizes the efficiency dependence on scanning angle spread for an $\alpha = 1$, $R_0 = 0.45$ cm beam. The efficiency is reduced by $\sim 15\%$ for a scanning-angle spread of 45°; the reduction increases to 50% for a scanning-angle spread of 90°. The TE_{121} mode is completely suppressed for scanning angles up to 90°. The relative magnitude of the TE_{121} mode grows rapidly as the scanning-angle spread is increased beyond 90°. The magnicon mode disappears completely for a spread of 180° and the TE_{121} mode reaches an efficiency of $\sim 16\%$.

IV Discussion and Conclusions

A fully nonlinear, time-dependent, multimode theory has been formulated for the magnicon output cavity. Proper phase averaging between the modes, and between the modes and the beam electrons, is critical to accurate mode competition calculations. In nonsynchronous interactions this is achieved by averaging with respect to electron entrance time and the orbit guiding center angle. The synchronous mode interaction is invariant with respect to these two averages; however, it is affected by scanning angle spread which is included via a third average over scanning angles. Calculations have been carried out to model a second-harmonic X-Band magnicon experiment which is currently underway at NRL. The calculations, although lengthy, can be feasibly carried out on a fast computer such as the Cray. The output cavity has been optimized for the TM_{210} mode at 11.4 GHz or twice the drive frequency ($\omega_d = 5.7$ GHz). The principal competing mode in this configuration is the TE_{121} mode. Nonsynchronous mode interactions are found to be suppressed by the synchronous interaction if the scanning angle spread is sufficiently small ($\leq 90°$ in the NRL configuration). Simulations of beam propagation in the deflection cavities suggest that the scanning angle spread at the output cavity in the NRL experiment will be less than this, so that mode competition in the output cavity is not expected to be a problem.

V Acknowledgment

The authors acknowledge many helpful discussions with Drs. Bahman Hafizi and Wallace M. Manheimer. This work was supported by the Department of Energy under Interagency Agreement No. DE-AI02-94ER40861.A000, and the Office of Naval Research.

References

[1] M. Karliner, E.V. Kozyrev, I.G. Makarov, O.A. Nezhevenko, G.N. Ostreiko, B.Z. Persov, and G.V. Serdobintsev, *Nucl. Instrum. Methods Phys. Res.*, **A269**, 459 (1988).

[2] V.E. Akimov, Yu.V. Baryshev, B.S. Estrin, M.M. Karliner, I.V. Kazarezov, E.V. Kozyrev, G.I. Kuznetsov, I.G. Makarov, O.A. Nezhevenko, G.N. Ostreiko, B.E. Persov, G.V. Serdobintsev, M.A. Tiunov, V.P. Yakovlev, and I.A. Zapryagaev, *Proceedings of the Second European Particle Accelerator Conference*, Nice, 1990, (World Scientific, Singapore, 1992) vol. 1, p. 1000.

[3] W.M. Manheimer, *IEEE Trans. Plasma Sci.*, **18**, 632 (1990).

[4] O.A. Nezhevenko, *Conference Record-1991 IEEE Particle Accelerator Conference*, edited by L. Lizama and J. Chew (Institute of Electrical and Electronic Engineers, New York, 1991), vol. 5, p.2933.

[5] B. Hafizi, Y. Seo, S.H. Gold, W.M. Manheimer, and P. Sprangle, *IEEE Trans. Plasma Sci.*, **20**, 232 (1992).

[6] S.H. Gold, C.A. Sullivan, B. Hafizi, and W.M. Manheimer, *IEEE Trans. Plasma Sci.*, **21**, 383 (1993).

[7] B. Hafizi, S.H. Gold, W.M. Manheimer, and P. Sprangle, *Phys. Fluids B*, **5**, 3045 (1993).

[8] O.A. Nezhevenko, V.P. Yakovlev, S. H. Gold, and B. Hafizi, *IEEE Trans. Plasma Sci.*, **22**, 785 (1994).

[9] O.A. Nezhevenko, *IEEE Trans. Plasma Sci.*, **22**, 756 (1994).

[10] D.E. Rees, *IEEE Trans. Plasma Sci.*, **22**, 773 (1994).

[11] B. Hafizi and S.H. Gold, "Optimization Studies of Magnicon Efficiency," *Phys. Plasmas*, to be published.

[12] A.W. Fliflet, R.C. Lee, S.H. Gold, W.M. Manheimer, and E. Ott, *Phys. Rev. A*, **43**, 6166 (1991).

[13] S.H. Gold, A.W. Fliflet, *Int. J. Electronics*, **72**, 779 (1992).

[14] A.W. Fliflet, *Int. J. Electron.*, **61**, 1049 (1986).

[15] A.W. Fliflet, M.E. Read, K.R. Chu, and R. Seeley, *Int. J. Electron.*, **53**, 505 (1982).

[16] A.W. Fliflet and W.M. Manheimer, *Phys. Rev. A*, **39**, 3432 (1989).

[17] *Handbook of Mathematical Functions*, ed. by M. Abramowitz and I.A. Stegun, (*Dover Publications, Inc.*: New York) chap. 25 (1970).

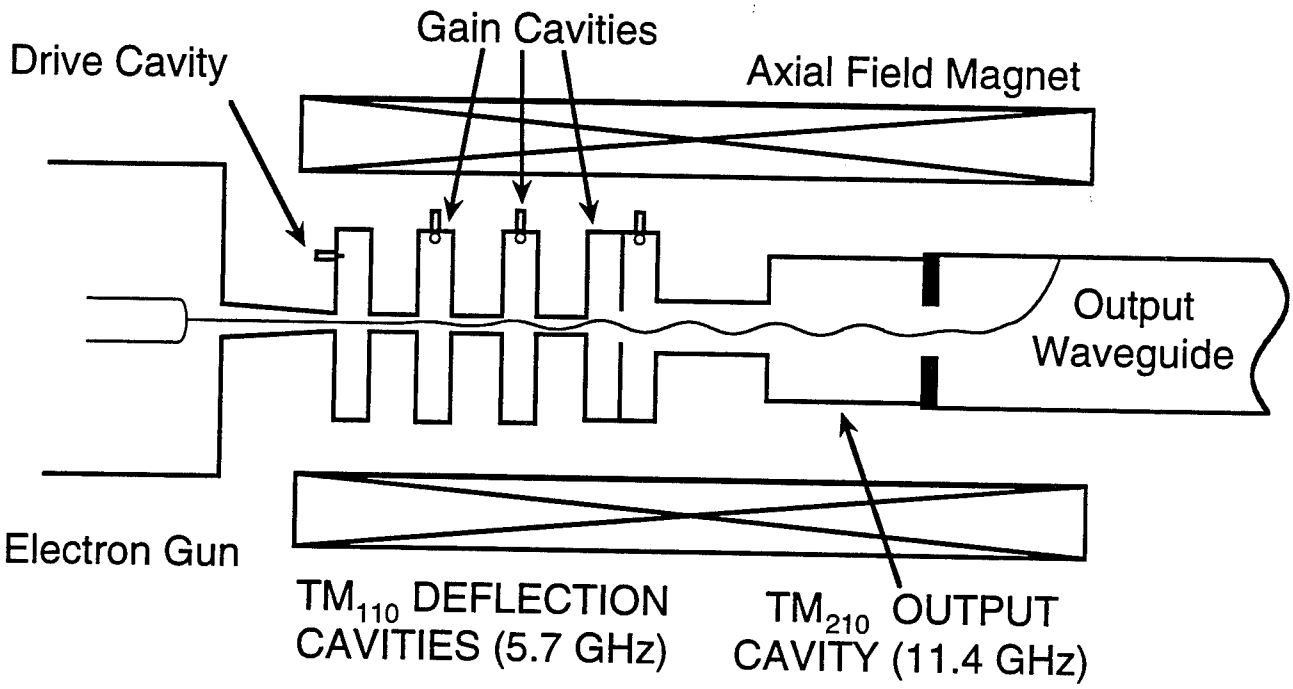

Fig. 1. Schematic of second harmonic magnicon amplifier.

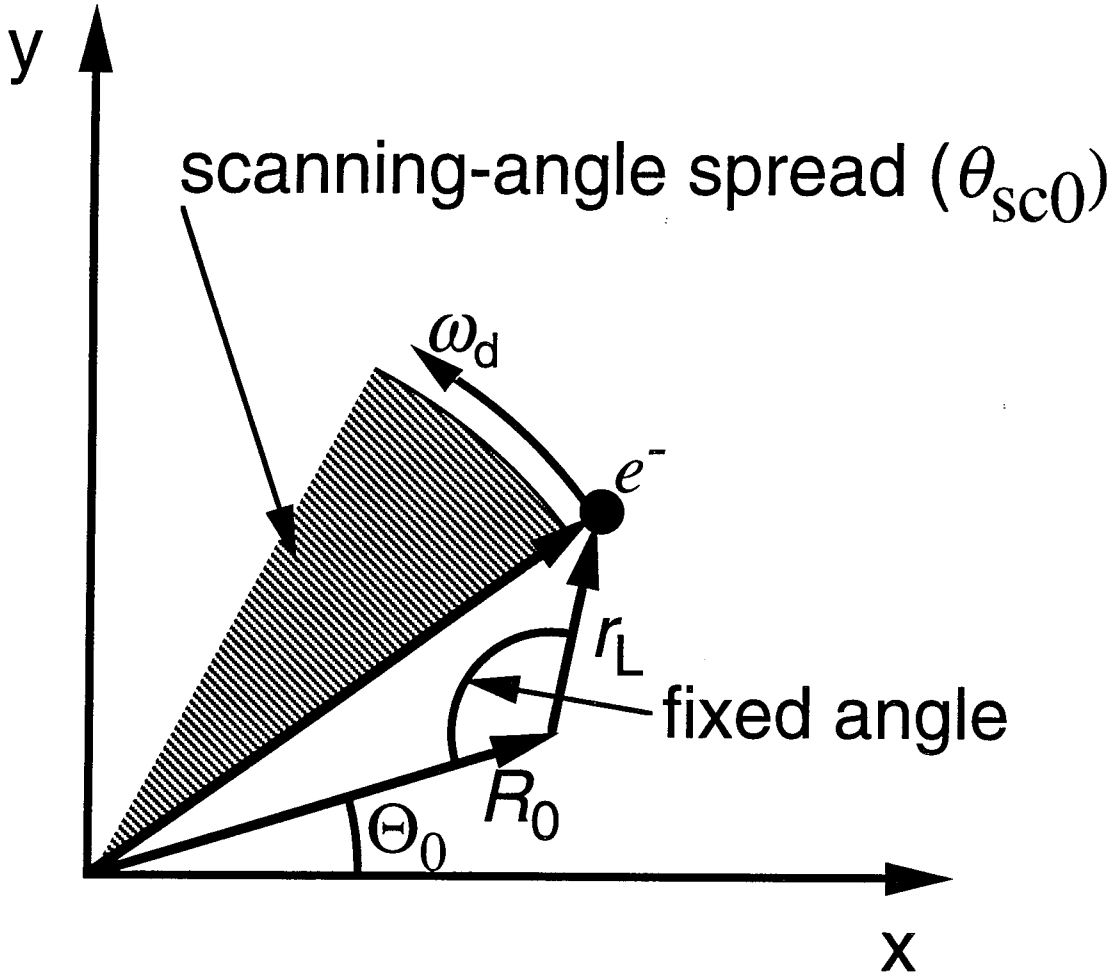

Fig. 2. Electron beam parameters at entrance to output cavity.

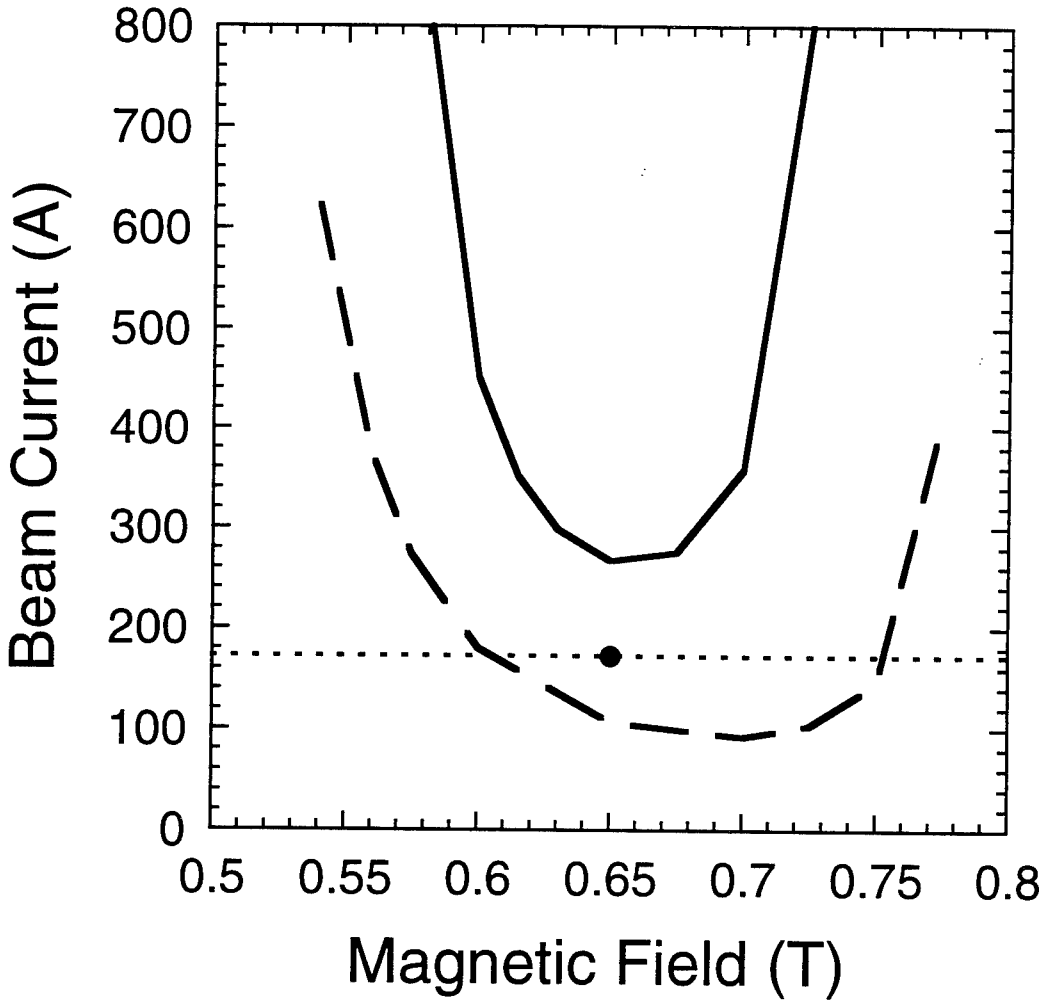

Fig. 3. Comparison of threshold oscillation currents for the TM_{210} and TM_{121} modes.

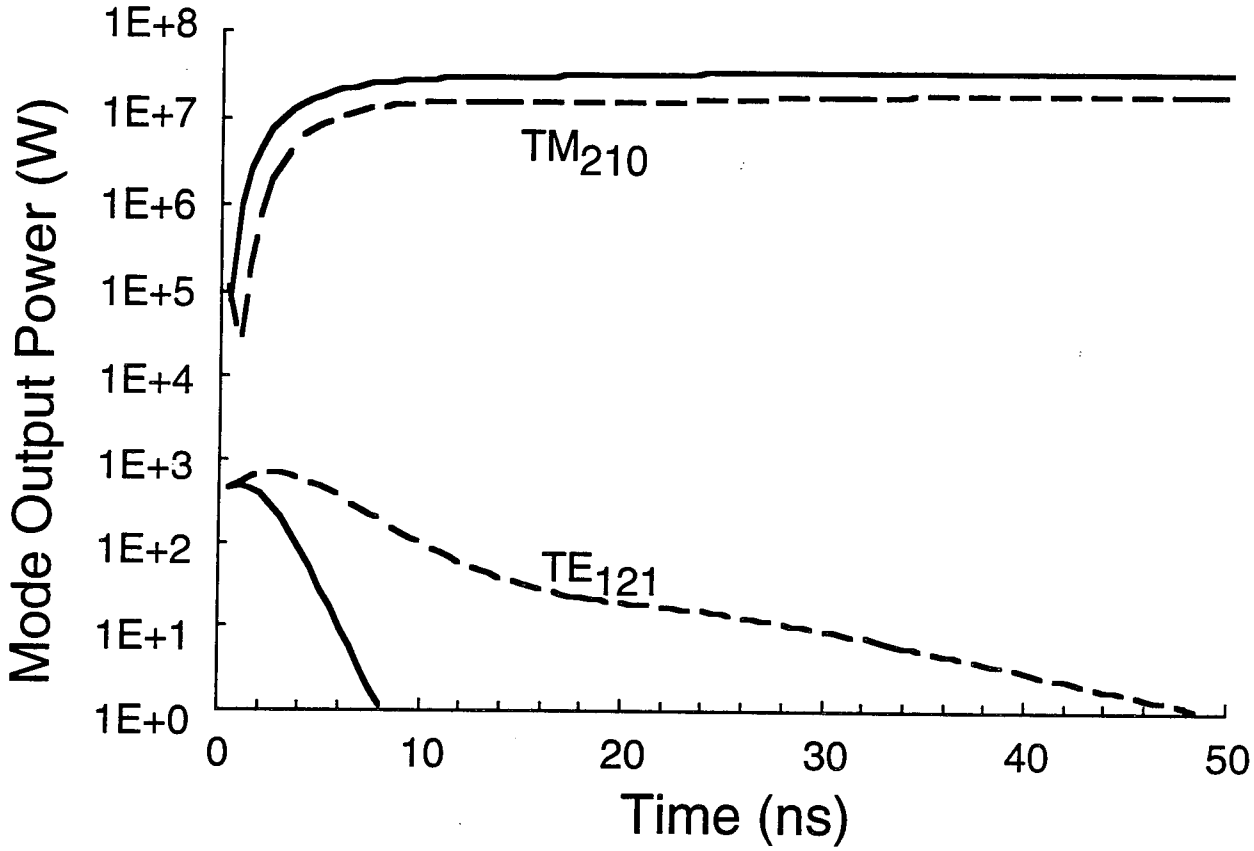

Fig. 4. Time evolution of the output power in the TM_{210} and TM_{121} modes. Solid curves: $\theta_{sc0} = 45°$, dashed curves: $\theta_{sc0} = 90°$.

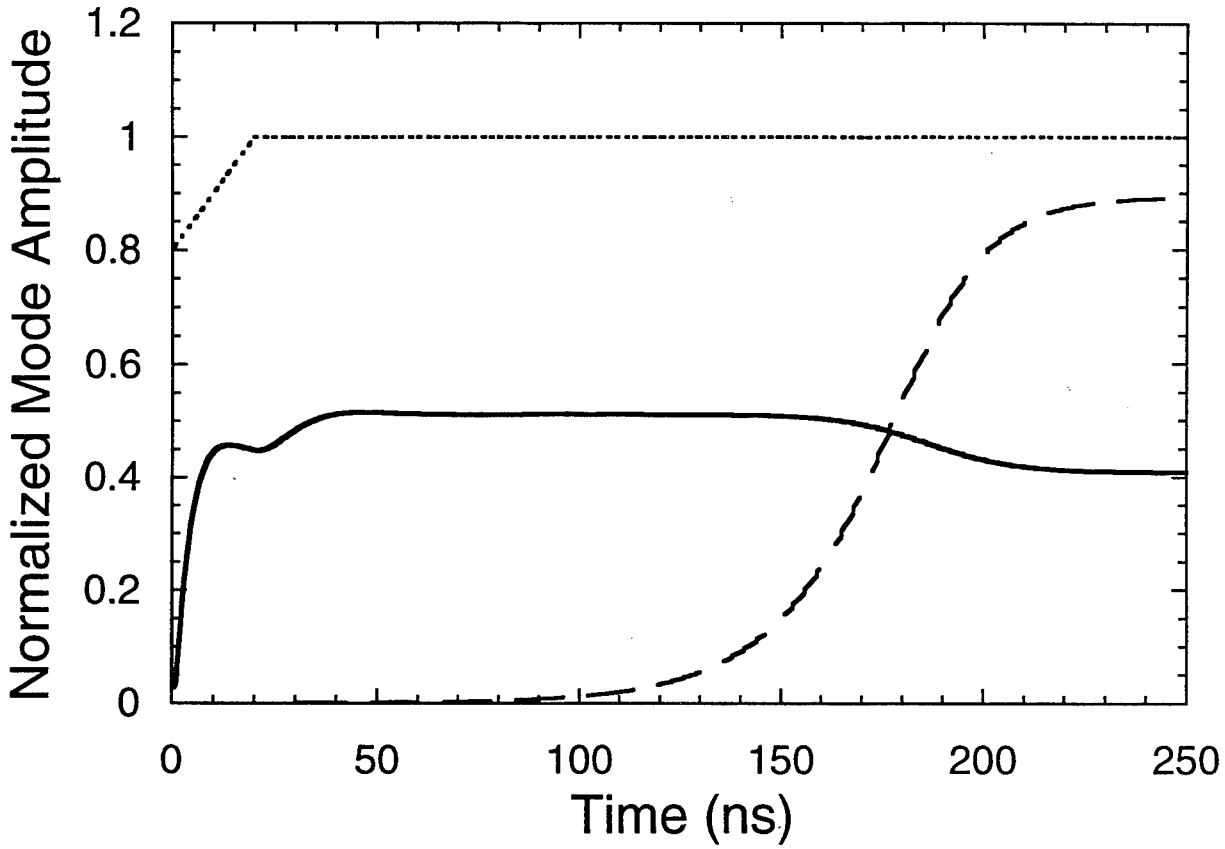

Fig. 5. Time evolution of the normalized mode amplitudes (f_m and f_g) for $\theta_{sc0} = 122°$. Solid curve: TM_{210} mode, dashed curve: TE_{121} mode, dotted curve: voltage profile.

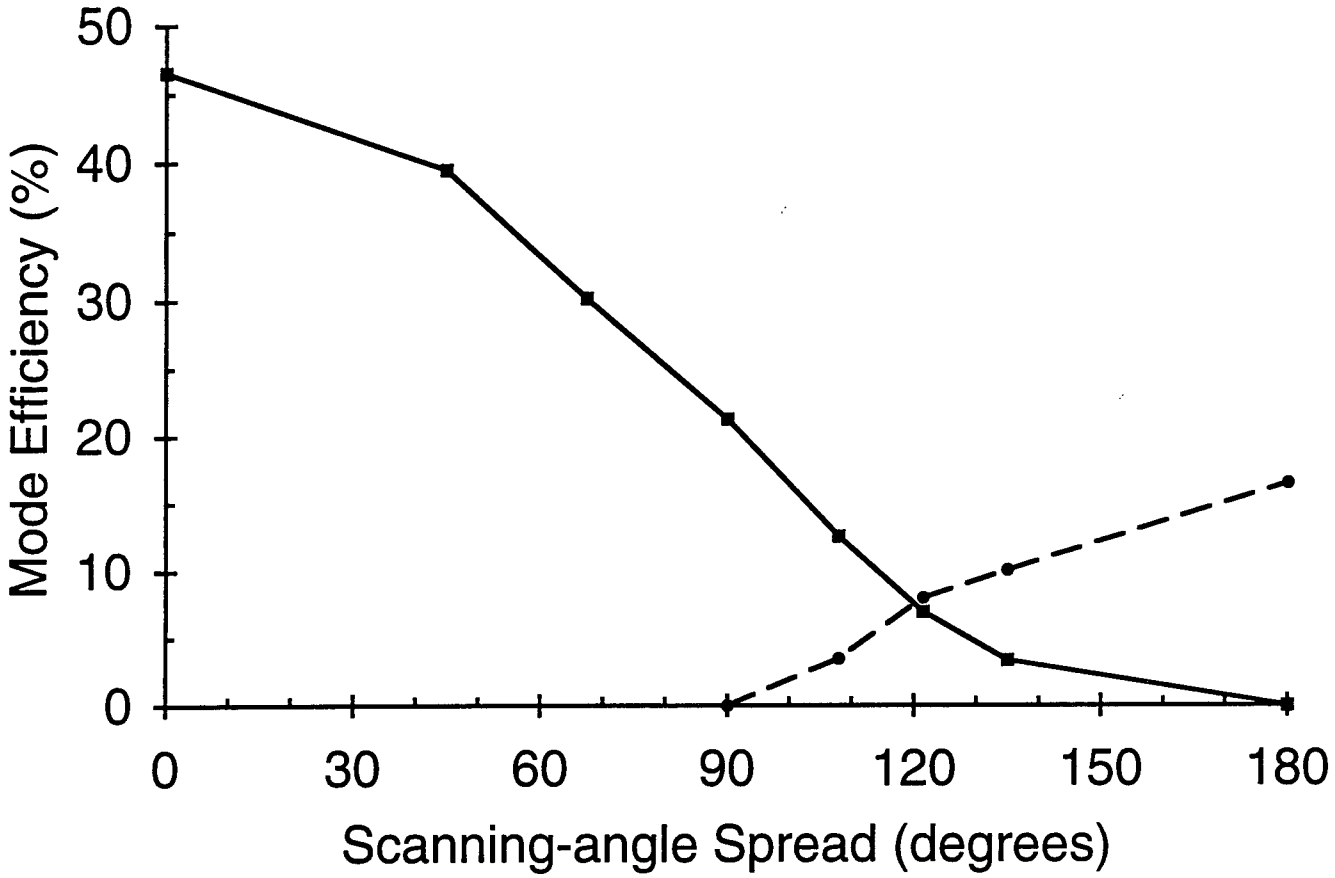

Fig. 6. Output efficiency for each mode as a function of scanning-angle spread. Solid curve: TM_{210} mode, dashed curve: TE_{121} mode.